ELSEVIER

Journal of Molecular Structure (Theochem) 500 (2000) 339–362

THEO CHEM

www.elsevier.nl/locate/theochem

Experimental and theoretical electronic charge densities in molecular crystals

G.U. Kulkarni, R.S. Gopalan, C.N.R. Rao*

Chemistry and Physics of Materials Unit, Jawaharlal Nehru Centre for Advanced Scientific Research, Jakkur P.O., Bangalore 560 064, India

Abstract

Electronic charge density distribution in molecular systems has been described in terms of the topological properties. After briefly reviewing methods of obtaining charge densities from X-ray diffraction and theory, typical case studies are discussed. These studies include rings and cage systems, hydrogen bonded solids, polymorphic solids and molecular NLO materials. It is shown how combined experimental and theoretical investigations of charge densities in molecular crystals can provide useful insights into electronic structure and reactivity.

Keywords: Electronic charge densities; Molecular crystals; Topological properties

1. Introduction

The description of charge distribution in crystalline lattices has come a long way since the first quantum model of the atom. It was known from early days that a quantitative account of the chemical bonds in molecules and crystals would require the calculation of the probability density of the electron cloud between atoms. The experimental possibility itself was considered soon after the discovery of X-ray diffraction. As early as 1915, Debye [1] stated "that experimental study of scattered radiation, in particular from light atoms, should get more attention, since along this way it should be possible to determine the arrangement of electrons in the atoms". Calculation of charge densities in molecules has been a preoccupation of theoretical chemists for sometime [2] and several charge density investigations of crystalline solids by both experiment and theory have been reported in the literature [3–11]. These comprise molecular crystals including non-linear materials, metallo-organic complexes and inorganic compounds. Koritsanszky [12] has provided a summary of charge density studies with reference to the topological properties and the electrostatic potential. The more recent literature has been surveyed by Spackman [13,14] and the charge density analysis in relation to metal–ligand and intermolecular interactions, has been discussed by Coppens [15].

In this article, we discuss electronic charge density in molecular systems as obtained from both experiment and theory. Besides introducing the topological analysis of charge density, we examine the experimental methods based on X-ray crystallography. In addition to dealing with the multipolar formalism for treating the experimental data, the program packages for orbital calculations in free molecules and crystals are mentioned. In particular, we discuss ring and cage systems, intermolecular hydrogen bonds, polymorphism and non-linear optical crystals.

* Corresponding author. Tel.: + 91-80-846-2762; fax: + 91-80-846-2766.

E-mail address: cnrrao@jncasr.ac.in (C.N.R. Rao).

0166-1280/00/$ - see front matter
PII: S0166-1280(00)00432-2

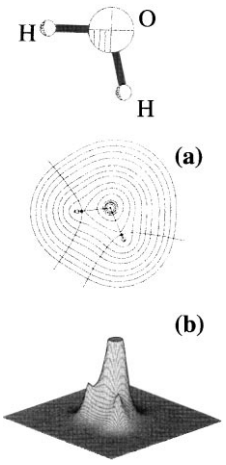

Fig. 1. Water: charge density in the molecular plane, (a) the contour map. The outermost contour has the value 0.0067 $e\text{Å}^{-3}$. The density increases almost exponentially for inner contours. The bond paths, the interatomic surfaces and the bond critical points are also indicated. (b) The relief map where the atom-cores are seen as peaks (reproduced with permission from Bader [2]).

2. Description of electronic charge density

The electronic charge density in an N-electron system is the probability per unit volume of finding any of the electrons in the phase space τ,

$$\rho(r) = N \int \psi^* \psi \, \mathrm{d}\tau \tag{1}$$

where ψ is the stationary state function; τ denotes the spin coordinates of all the electrons and the Cartesian coordinates of all N electrons but one [2]. It is expressed in $e\text{Å}^{-3}$ or au (1 au = 6.7483 $e\text{Å}^{-3}$). The description of electronic structure of a molecule in real space therefore relates to the charge density distribution around the constituent atoms. The density in a molecule can be conveniently modeled by partitioning into core, spherical valence and deformation valence around each atom [16],

$$\rho_{\text{atom}}(r) = \rho_{\text{core}}(r) + \rho_{\text{valence}}(r) + \rho_{\text{deformation}}(r, \theta, \phi) \tag{2}$$

The topology of a charge distribution has many rich features—maxima, minima, saddles and nodes which help characterize intuitional elements such as atom cores, bonds and lone-pair electrons. As an example, the charge density distribution in water molecule [2] is depicted in Fig. 1 in the form of contour as well as relief maps. The density is maximum at the oxygen core position and decreases steeply towards the mid-region between oxygen and hydrogen reaching the minimum value at the 'critical point' ($\nabla\rho = 0$). This point carries maximum densities from the other two perpendicular directions. A quantitative description of charge density thus boils down to examining the number and the nature of such critical points in and around a molecule. A critical point (CP) is characterized not only by its density and location but also by the curvatures and the associated signs. The curvature of charge density at a point ($\nabla^2\rho$) well known as the Laplacian, is a measure of the charge concentration ($\nabla^2\rho < 0$) or depletion ($\nabla^2\rho > 0$) at that point. It is obtained as the sum of eigenvalues—λ_1, λ_2 and λ_3 of the Hessian matrix diagonalized against principal axes of curvature with λ_3 set along the internuclear vector. The rank of the matrix (3 for a stable molecular system) and the signature (sum of the signs of eigenvalues) imply the nature of the critical point. At a (3, −3) CP, for example, all the curvatures are negative and ρ is locally the maximum. All the atom-cores exhibit (3, −3) CPs in ρ (see Table 1). The relative magnitudes of the curvatures perpendicular to the bond direction (λ_3) determine the ellipticity [17] associated with a bond, $\epsilon = (\lambda_1/\lambda_2) - 1$.

An estimate of bond polarization [17] can be obtained from the location of the bond CP with respect to the internuclear vector,

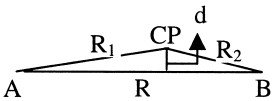

$$\Delta_B\% = 100 \times (R_m - R_1)/R_m$$

Table 1
Critical points in molecular systems

Function	CP (rank, signature)	Chemical entity
$\rho(r)$	(3, −3)	Atom
$\rho(r)$, $V(r)$	(3, −1)	Bond
$\rho(r)$	(3, +1)	Ring
$\rho(r)$	(3, +3)	Cage
$\nabla^2\rho(r)$	(3, −3)	Lone-pairs
$V(r)$	(3, +3)	Lone-pairs

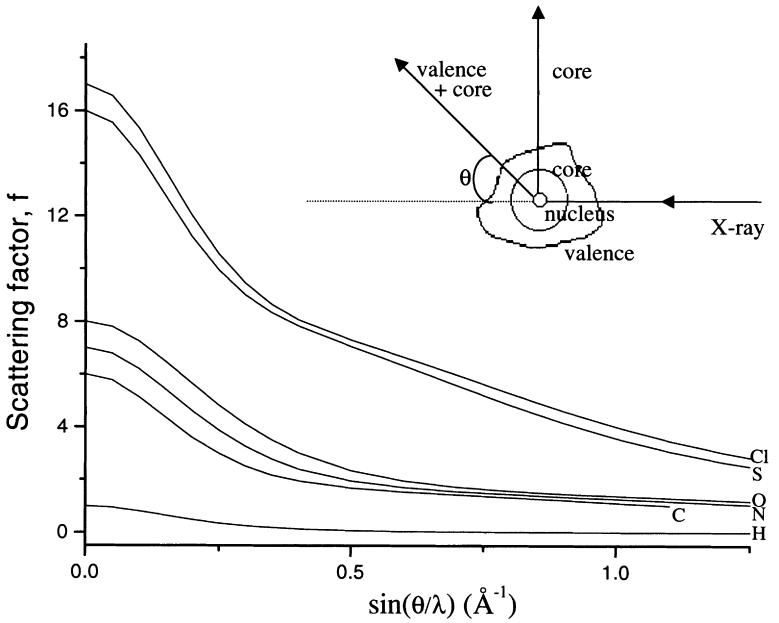

Fig. 2. Variations of the scattering factor with sin θ/λ for different atoms. Above 0.5 Å^{-1}, the scattering due to valence electrons decreases gradually and the atom-core becomes visible. This is shown schematically in the inset. The scattering factors were obtained from the International Tables for Crystallography, Vol. IV, (1974) p. 71.

$$\Delta_B\% = 100 \times (R_m - R_1)/R_m \quad (3)$$

where $R_m = (R_1 + R_2)/2$. The Δ value is used to describe relative electronegativities of the atoms involved. The strain involved in a bond can be estimated [17] in terms of the vertical displacement, d of the bond path from the internuclear vector

$$d = 2 \times \sqrt{s \times (s - R_1) \times (s - R_2) \times (s - R)}/R \quad (4)$$

where $s = (R_1 + R_2 + R)/2$.

The electrostatic potential [18,19] generated by a molecule containing nuclear charges, z_i, placed at R_i, with a charge distribution $\rho(r)$, is given by

$$V(r) = \sum_i \frac{z_i}{|r - R_i|} - \int \frac{\rho(r')}{|r' - r|} d^3r' \quad (5)$$

It is more useful in describing attractive and repulsive interactions and also in determining the electrophilic and nucleophilic sites in molecules. The other quantity of interest is the kinetic energy density at the critical point, G_{CP} [20] which has been obtained by

$$G_{CP} = \frac{3}{10}(3\pi)^{2/3}\rho_{CP}^{5/3} + \frac{\nabla^2\rho_{CP}}{6} \quad (6)$$

This quantity has been used in some cases for the calculation of hydrogen bond energies [21] and their classification [22].

3. Charge density from X-ray diffraction

Experimental determination of charge density relies mostly on X-ray diffraction although other techniques have been applied in some instances. X-ray diffraction arises from scattering by electrons and therefore carries information on the distribution of electronic charge in real space [10]. The intensity of a Bragg reflection, $I(\mathbf{h})$, at a given temperature, is proportional to the square of its structure factor,

$$I(\mathbf{h}) \propto |F(\mathbf{h})|^2 \propto \left| \sum_i f_i(\mathbf{h})\, e^{2\pi i \mathbf{h}\cdot\mathbf{r}} \right|^2 \quad (7)$$

where $f_i(\mathbf{h})$ is the scattering factor of the ith atom in

the unit cell of volume, V. The charge density is obtained by the Fourier summation of the experimentally measured reflections

$$\rho(r) = \frac{1}{V}\sum_{\mathbf{h}} F(\mathbf{h})\, e^{-2\pi i \mathbf{hr}} \tag{8}$$

In conventional structure determination, $f_i(\mathbf{h})$ is approximated to the scattering factor from spherical electronic density, while for a complete description of bonding, accurate modeling of $f_i(\mathbf{h})$ becomes necessary. In parallel to $\rho(r)$ (see Eq. (2)),

$$f(\mathbf{h}) = f_{\text{core}}(\mathbf{h}) + f_{\text{valence}}(\mathbf{h}) + f_{\text{deformation}}(\mathbf{h}) \tag{9}$$

Such a partitioning of $f(\mathbf{h})$ is justifiable in X-ray diffraction since one can select regions of reciprocal space where core scattering is predominant. In Fig. 2, we show variation of $f(\mathbf{h})$ with scattering angle, θ, for various elements. Each curve is composed of two regions. At low angles or Bragg vector ($\mathbf{h} = 2\sin\theta/\lambda$), $f(\mathbf{h})$ decreases steeply and above $\sim$0.5 Å^{-1}, the fall is gradual. The first part has contributions from both the atom-core and the valence density while the second arises mainly due to the core. Thus, X-ray diffraction facilitates extraction of the bonding or the deformation density,

$$\rho_{\text{deformation}} = \rho_{\text{total}} - \rho_{\text{promolecule}} \tag{10}$$

where promolecule is obtained by the superposition of atoms without any interaction between them. This is called the (X–X) method. In the (X–N) method, the core positions along with the thermal parameters are obtained from a neutron diffraction experiment. The latter is particularly useful while dealing with hydrogen atom positions though it requires two data sets, which can be expensive besides having to grow bigger crystals. In recent years, the (X–X) method has become more popular.

Eq. (8) above necessitates data collection covering a wide range of the reciprocal space. For small unit cells with dimensions $\sim$30 Å, data collection up to moderately high resolution (1.25 Å^{-1}) can be achieved using short wavelength radiations such as MoK$_\alpha$ (0.71 Å). Moreover, data collection strategy critically depends on the type of the diffractometer. In the past, point detectors mounted on a four circle diffractometers were used for charge density measurements with the data collection extending in some cases to a period of few weeks. Of late, area detectors or image plates are preferred over the conventional ones, as the experiments can be carried out faster with greater redundancy [23]. Area detectors in combination with synchrotron radiation are becoming increasingly popular [24,25]. Koritsanszky et al. [25] demonstrated that the charge density data can be collected within a day.

Thermal smearing of the charge density caused by atomic vibrations can hamper the extraction of subtle features of bonding,

$$f(T)|_{(h,k,l)} = f(0)\exp\left(-(b_{11}h^2 + b_{12}hk + b_{13}hl + b_{22}k^2 + b_{23}kl + b_{33}l^2)\right) \tag{11}$$

where

$$2\pi^2 a^{*2}U_{11} = b_{11} \qquad 2\times 2\pi^2 a^* b^* U_{12} = b_{12} \qquad \text{etc.}$$

where U_{ij}s are the anisotropic displacement parameters and a^*, b^* and c^* are the reciprocal lattice vectors. Low temperature experiments at $\sim$100 K, are carried out by allowing a stream of liquid nitrogen to fall on the crystal. In some cases however, much lower temperature ($\sim$20 K) has been achieved using one or two stage He-closed-cycle cryostats [9]. It is also necessary to choose a good quality, least mosaic crystal for charge density work.

4. Data refinement and computer codes

A preliminary knowledge of the crystal structure is important prior to a detailed charge density analysis. Direct methods are commonly used to solve structures in the spherical atom approximation. The most popular code is the SHELX from Sheldrick [26] which provides excellent graphical tools for visualization. The refinement of the atom positional parameters and anisotropic temperature factors are carried out by applying the full-matrix least-squares method on a data corrected if found necessary, for absorption and diffuse scattering. Hydrogen atoms are either fixed at idealized positions or located using the difference Fourier technique.

In the absence of inputs from neutron diffraction, a higher-order refinement of X-ray data (>0.6 Å^{-1}) becomes essential to obtain accurate core positions and the associated thermal parameters (the X–X

method). In this case, the hydrogen atom positions are often adjusted to the average neutron diffraction values [27] and are held there during the refinement. Often, the rigid bond test [28] is carried out and the parameters are corrected for translation–libration motions of the molecule [29]. The aspherical atom electron density is obtained in a local coordination system using the Hansen–Coppens formalism [16],

$$\rho(\mathbf{r}) = \rho_c(r) + P_v\rho_v(\kappa r) + \sum_l R_l(\kappa' r) \sum_{m=-l}^{l} P_{lm} y_{lm}\left(\frac{\mathbf{r}}{r}\right) \tag{12}$$

Here, ρ_c and ρ_v are the spherically averaged Hartree–Fock core and valence densities, respectively, with ρ_v normalized to one electron. The Slater type radial functions $R_1 = N_1 r^n \exp(-\kappa' \xi r)$, modulated by the multipolar spherical harmonic angular functions y_{lm} define the deformation density. The population parameters, P_v and P_{lm}, are floated along with κ, κ' during the refinement. The kappa parameters control the expansion or the contraction of the radial part of the electron cloud with respect to the free atom. The multipoles on the first row atoms are generally refined up to octapole moments, while for the heavier ones, moments up to hexadecapole are used. Hydrogen atoms are restricted to dipole, although occasionally quadrupole moments are included in the refinement. The above formalism is well adopted in the recently developed user-friendly program package, XD [30]. Older codes such as MOLLY [16], VALRAY [31], LSEXP [32], POP [33] are also still in use. The quality of a refined model can be monitored based on the residuals and the goodness-of-fit apart from closely inspecting the deformation density maps.

The valence population coefficients P^i can be used to estimate the pseudo-atomic charges on the different atoms according to the equation,

$$q_i = n_i - P^i_{\text{core}} - P^i_{\text{valence}} \tag{13}$$

where n_i is the total number of electrons of atom i. The molecular dipole moment is given by

$$\mathbf{p}_i = \sum_i z_i \mathbf{R}_i + \int_v \mathbf{r}\rho_i(\mathbf{r}_i)\, d\mathbf{r} \tag{14}$$

5. Theoretical methods

Electronic charge density distribution in a molecule or a crystal may be obtained by Hartree–Fock calculations [34]. It involves calculation of antisymmetrized many-electron wavefunction and minimizing the energy with respect to the coefficients of the one-electron wave function. When the energy is minimized, the wavefunction is said to have achieved self-consistency (SCF). Slater type atomic orbitals were used in the past which posed lot of difficulty in analytically integrating the polynomial functions. Use of gaussian functions in the radial part of the wavefunction has made HF method more applicable. Pople [35] has described the current status of ab initio quantum chemical models in his recent Nobel lecture. The accuracy that can be reached with these models critically depends on how many gaussians, polarization and diffuse functions make the basis set. In principle, using a full configuration interaction (FCI) with a large number of gaussians on each orbital should give the best results. For example, calculations performed using 6-311G**++ basis sets at FCI level of theory is common with small molecules. Computer program packages like GAUSSIAN [36] and GAMESS [37] are available for ab initio calculations on molecules. MOPAC [38] is used at a semi-empirical level. Periodic Hartree–Fock calculations suitable for crystalline substances has been incorporated in CRYSTAL algorithm by Dovesi et al. [39]. It uses one-particle basis function made up of Bloch functions,

$$\chi_i(r,k) = (1/\sqrt{N}) \sum_t \chi_a^t \, e^{ikt} \tag{15}$$

Here χ_a^t refers to the ath atomic orbital in the unit cell of the crystal described by the lattice translation vector, t. The CRYSTAL code is also capable of calculating charge density in a solid using the density functional theory (DFT) at local density approximation (LDA) or at generalized gradient approximation (GGA).

The charge density obtained using the theoretical procedures can be usefully compared with that from X-ray diffraction by several means. Charge density maps either in total or in deformation provide the obvious tools to evaluate how well the two models agree. CRYSTAL95 [39] offers routines to calculate

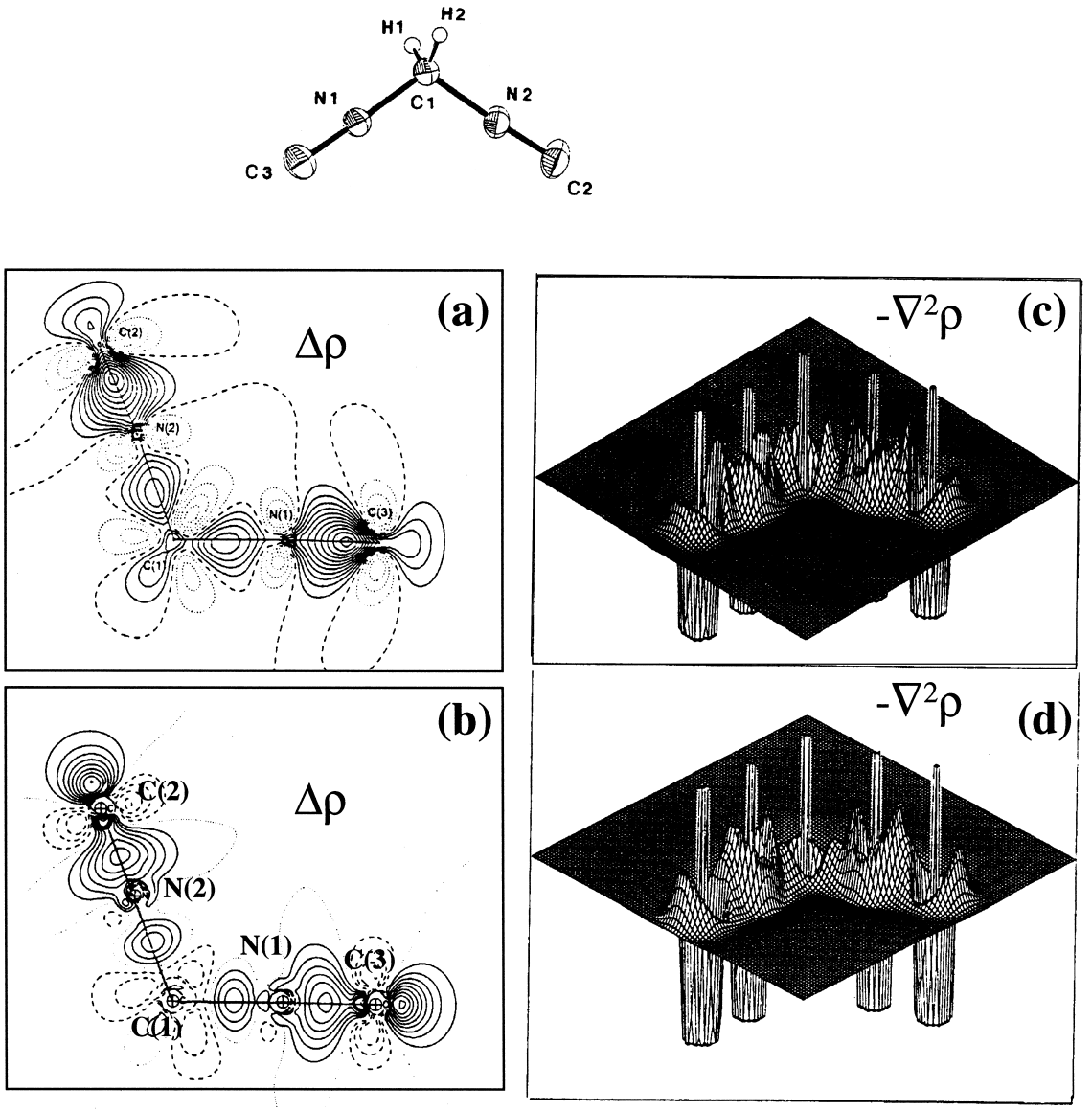

Fig. 3. Charge density in diisocyanomethane: deformation density maps in the molecular plane (a) experimental (b) theoretical (contours at 0.1 eÅ^{-3}). The non-bonded regions of C(2) and C(3) are more depleted in (a) with the density migrating to the inside of the molecule. The corresponding Laplacians (range −20 to 250 eÅ^{-5}) are shown in (c) and (d), respectively (reproduced with permission from Koritsanszky et al. [40]).

X-ray structure factors from the theoretical density. Using the theoretical structure factors, one can carry out multipolar refinement in parallel to experimental X-ray data and make in depth comparison of the topological properties from the two sets.

6. Charge density in bonds, rings and cages

Covalent bonds are associated with high charge densities (1.5–3 eÅ^{-3}) and negative Laplacians, while ionic bonds are characterized by small densities and positive Laplacians. Hydrogen bonds are

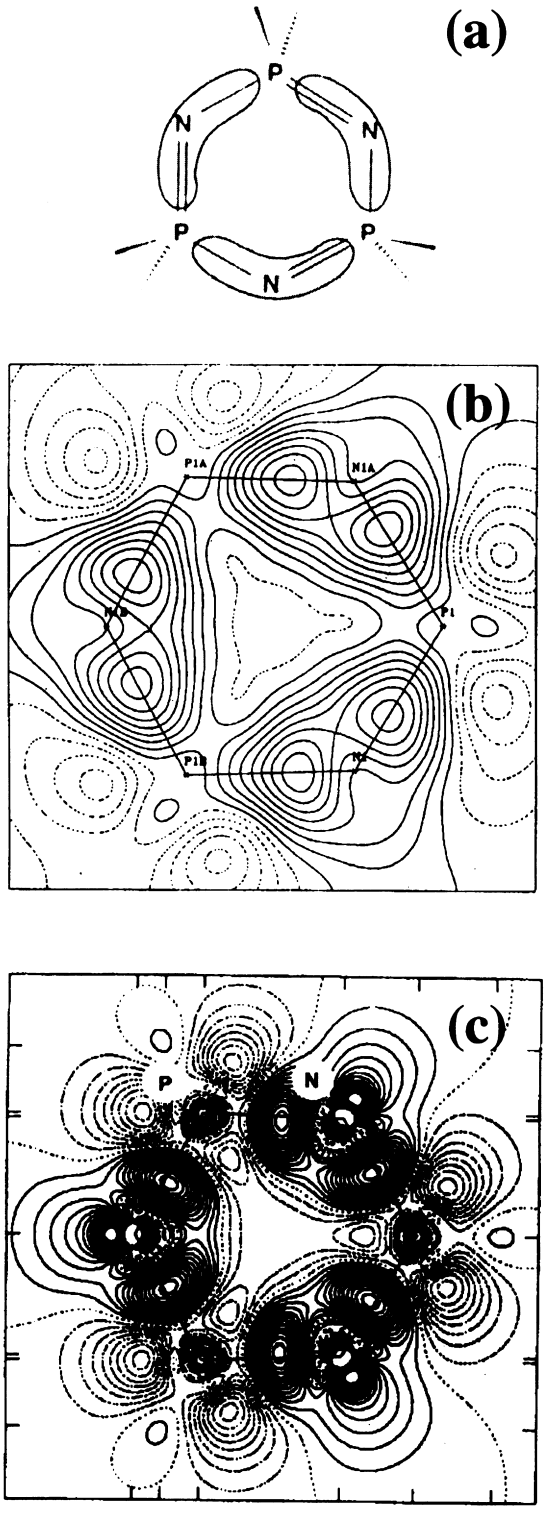

associated with even smaller densities and Laplacians. Following Cramer and Kraka [17], the charge density at critical point, ρ_{CP}, is a measure of the bond strength in covalent bonds. Thus, a typical C–C bond carries a density of $\sim 1.7\ e\text{Å}^{-3}$ at the CP while a C=C bond exhibits much higher density $\sim 2.5\ e\text{Å}^{-3}$. Similarly, the density associated with a C≡C bond is $\sim 2.8\ e\text{Å}^{-3}$. The ellipticity of a bond, ϵ, is a measure of its extent of double bond character. For cylindrically symmetric bonds, the ellipticity is therefore zero, while in the case of ideal carbon double bonds, the theoretical estimate gives $\epsilon \sim 0.74$. These quantities, in combination with bond polarity (Δ), pseudo-atomic charges and the bent bond character (d) describe a bond quantitatively.

Let us examine the case of diisocyanomethane as a typical example. Isocyanides possess a formally divalent carbon atom with a coordination number of only one. Though they are divalent, their bond lengths are only slightly longer than ideal C≡N bond and therefore a resonance is expected. Koritsanszky et al. [40] analyzed topographs of electron density of diisocyanomethane (Fig. 3) derived from both experiment and theory. Refinements of the experimental data were carried out with different levels of constraints. The most restricted model contained C_{2v} symmetry on the tetrahedral carbon (C1), rotational symmetry on isocyano groups and thermal motion correction on all non-hydrogen atoms. This model gave the best convergence for the data. They also carried out ab initio calculations at the Hartree–Fock and MP2 levels, optimizing the molecule with 6-311++G(3d,3p) basis sets starting from X-ray structural data. Fig. 3 shows the deformation density and the Laplacians in the mean molecular plane from both theory and experiment. There is a striking difference between the two deformation density maps in that the interatomic regions of the experimental map are richer in electron density at the expense of charge in the non-bonded regions of the terminal carbon atoms

Fig. 4. The phosphazene ring: (a) island delocalization model predicting nodes in π-density at the phosphorus atoms (b) dynamic deformation density (at $0.1\ e\text{Å}^{-3}$) in the plane of the ring (c) theoretical deformation density (at $0.05\ e\text{Å}^{-3}$) of cyclic phosphazene was used as a model (reproduced with permission from Cameron et al. [43]).

(compare Fig. 3a and b). The isocyano bonds are also more polarized. The same is reflected in the Laplacians shown in Fig. 3c and d, where bonded charge concentration appears as a sharp peak in the experimental map. This has been taken to indicate a greater swing of the NC bond resonance towards the N≡C bond.

Intramolecular bonding in benzene, triazine, phosphazene and such cyclic systems are of interest because of the varying degree of superposition of the s, p and d orbitals as the case may be. The Hückel rule predicts benzene to be aromatic with the π-electrons delocalized over the ring. According to the island delocalization model [41] for the phosphazene ring, the overlap of the d orbitals on the phosphorus atoms and the p orbitals on the nitrogen atoms in the ring would produce a π-system above and below the plane of the ring with nodes at each phosphorous atom (Fig. 4a). An extension of the π-system within and in the plane of the ring is also expected based on the π/π′ model due to Craig and Paddock [42]. Cameron et al. [43] applied charge density methods to study small cyclic systems. For this purpose, they carried out high resolution X-ray diffraction at 200 K with MoK_α radiation on hexaazirdinylcyclo-triphosphazene crystallized from benzene. This system is particularly interesting in that, the solvent benzene gets securely trapped between two phosphazene molecules and offers one to use it as an internal standard. They observed that the benzene ring in plane density was symmetric with respect to the carbon–carbon bonds while the density in a plane perpendicular to the ring across the center of a bond showed elongation in the direction of the π-system as expected. In contrast, the in-plane density in phosphazene was highly polarized as shown in Fig. 4b. Nodes in density at phosphorus atoms can be clearly seen from the figure. The electron density appears to spread from one P–N bond through the nitrogen to the second N–P bond as predicted by the island delocalization model. Further, there is a considerable spread of electron density inside the ring validating the π′-bonding model. Theoretical electron densities determined from ab initio calculations using GAMESS [37] with 6-31G* basis set depict similar features in the deformation density (see Fig. 4c).

Charge density distribution in cage rings has been investigated in few cases. An adduct of C_{60} was studied by Irngartinger et al. [44] who discussed the degree of aromaticity. These workers have also carried out charge density measurements on a cubane derivative, methyl 3,4-difluorocubane-1-carboxylate [45]. This compound with the fluorine substituents fixed in a *cis*-like orientation to the rigid cubane cage (see Fig. 5) was expected to serve as a model for the *cis* isomer of 1,2-difluoroethylene. The latter along with its cousins such as *gauche*-1,2-difluoroethane is known to be energetically favorable compared to the *trans* isomer (*anti* conformer). Wilberg and co-workers [46] explained this '*cis*/*gauche* stability effect' and predicted the C–C bond to be bent due the strongly electronegative property of the fluorine substituents. Difference density maps in various diagonal planes of the cubane indeed show bending of the C–C bonds (Fig. 5). The CF–CF bond and the CH–CF bonds were found to be more bent ($d \sim 0.16$ Å) than the CH–CH bonds ($d_{\text{average}} \sim 0.12$ Å). This study clearly provides an evidence that strong electronegative substituents increase the bending of the bonds to which they are attached.

7. Charge density of hydrogen bonds

Hydrogen bonds can be classified on the basis of charge density. Alkorta and co-workers studied various types of hydrogen bonds including dihydrogen bonds [47], bifurcated hydrogen bonds [48], H···π interactions [49], inverse H bonds [50] and hydrogen bonds involving carbenes and silylenes as acceptors [51]. In general, the hydrogen bond CPs are associated with small densities and positive Laplacians characteristic of closed-shell interactions. Zhang et al. [52] carried out theoretical studies on hydrogen bonded complexes, with strained organic systems like tetrahedrane acting as pseudo-π-acceptors while Larsen and co-workers [53,54] have studied the strong hydrogen bond in methylammonium hydrogen maleate and benzoylacetone. Such strong bonds arise due to shared interactions exhibiting relatively large density ($\sim 1\ e\text{Å}^{-3}$) and negative Laplacians ($-7\ e\text{Å}^{-5}$) like typical intramolecular bonds. They also find a ring critical point (3, +1) near the center of the keto–enol dimer in benzoylacetone. Experimental charge density study of *cis*-$HMn(CO)_4PPh_3$

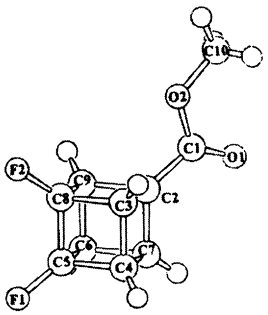

Methyl 3,4-difluorocubane-1-carboxylate

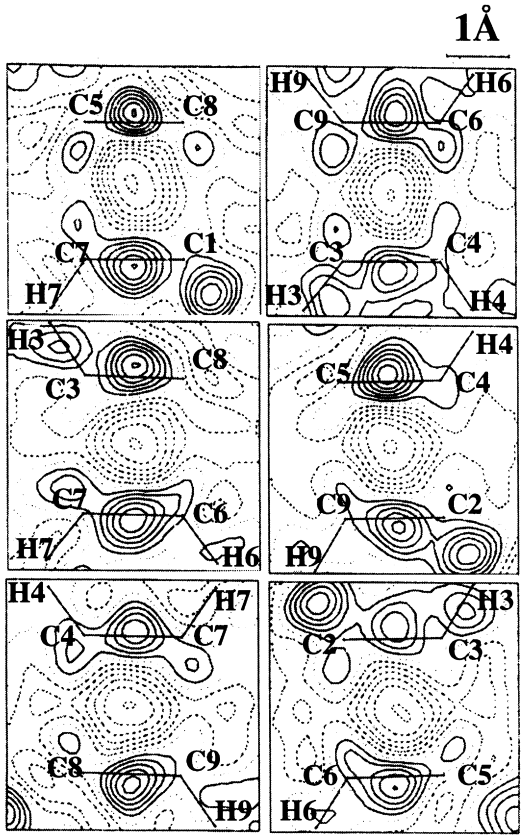

Fig. 5. Methyl 3,4-difluorocubane-1-carboxylate: difference density maps in various diagonal planes of the cubane cage. The maxima of the bond densities lie outside, implying that the cage bonds are bent (reproduced with permission from Irngartinger et al. [45]).

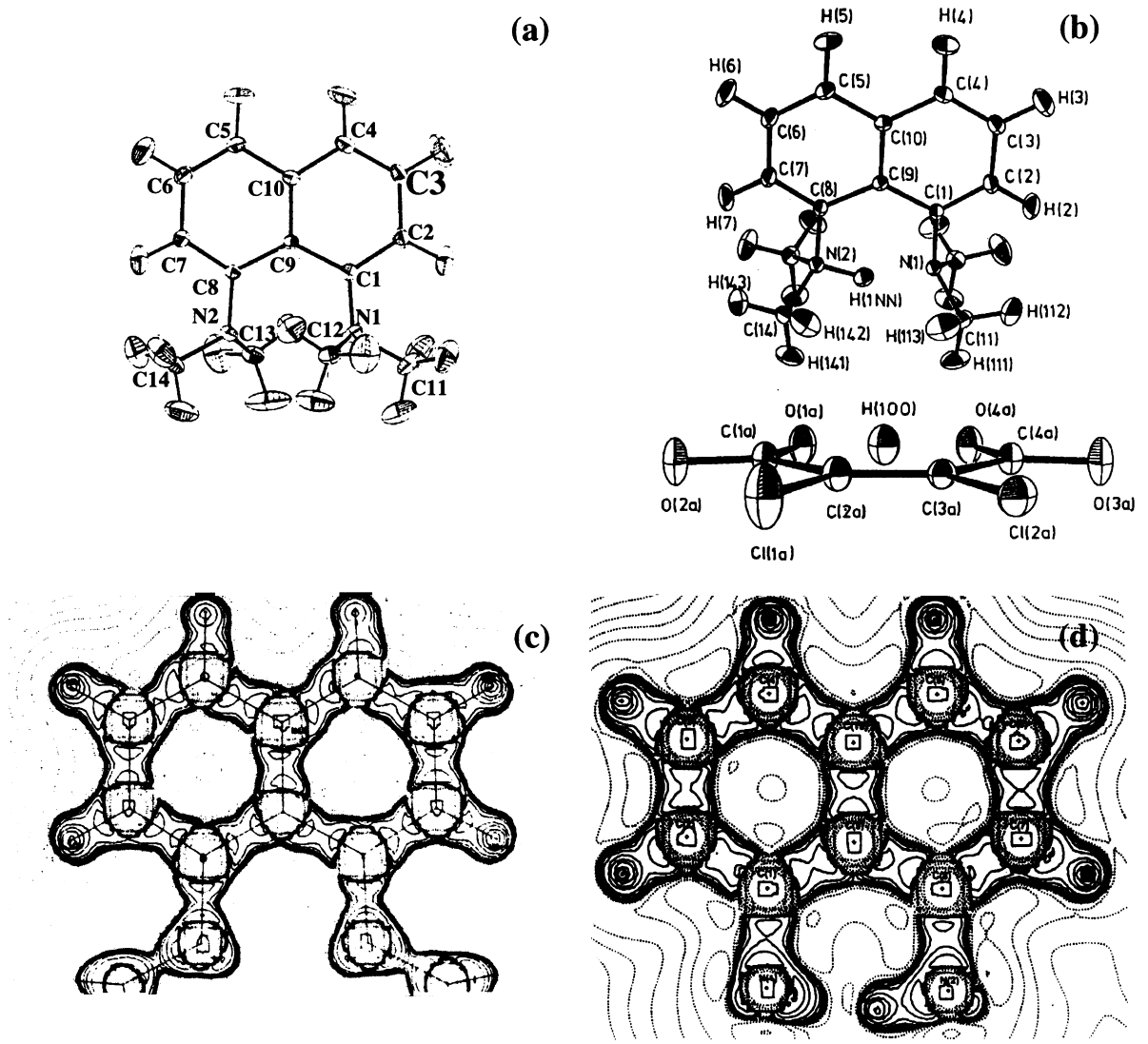

Fig. 6. A proton-sponge: (a) 1,8-Bis(dimethylamino)napthalene in the pristine form; (b) after protonation using 1,2-dichloro maleic acid. The contour maps of the corresponding Laplacians are shown at logarithmic intervals in (c) and (d), respectively (reproduced with permission from Mallinson et al. [56,57]).

has provided evidence for the C–H···H–Mn bond [55]. They found that the hydrogen atom in the Mn–H bond is nucleophilic carrying a charge of $-0.4e$ while that in the C–H is electrophilic ($0.3e$). The electrostatic part of the H···H interaction energy was estimated to be 5.7 kcal/mol, which is in the range of H-bond interactions. It is characterized by a critical point carrying a small density ($0.066\,e\text{Å}^{-3}$) and a positive Laplacian ($0.79\,e\text{Å}^{-5}$), somewhat higher compared to a typical C–H···O interaction.

Mallinson et al. [56,57] have carried out experimental and theoretical charge density determinations on a proton sponge compound, bis(dimethyamino)-napthalene (DMAN), in both pristine and protonated forms (Fig. 6). They used positional and thermal parameters of hydrogen atoms from an independent neutron diffraction experiment and treated the thermal

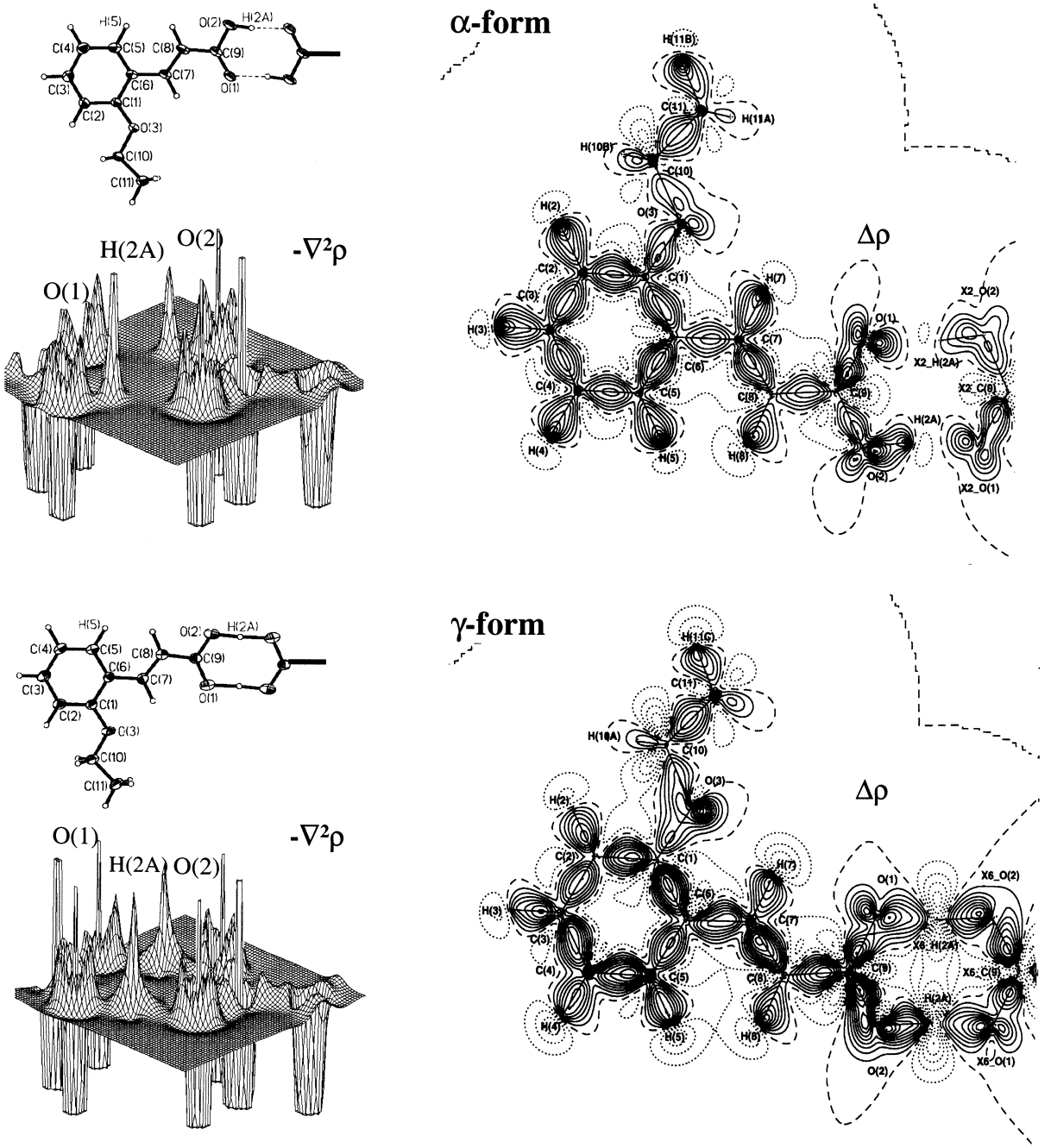

Fig. 7. Polymorphic forms of *o*-ethoxy cinnamic acid: molecular diagrams and deformation density maps close to the mean plane of the molecules in the α- and the γ-forms (contours at 0.12 eÅ^{-3}). Subtle differences in the cinnamoyl bond and the hydrogen bond region are noticeable. The Laplacians of the intermolecular hydrogen bonds in the acid dimer are shown in the relief maps along side (range −250 to 250 eÅ^{-5}).

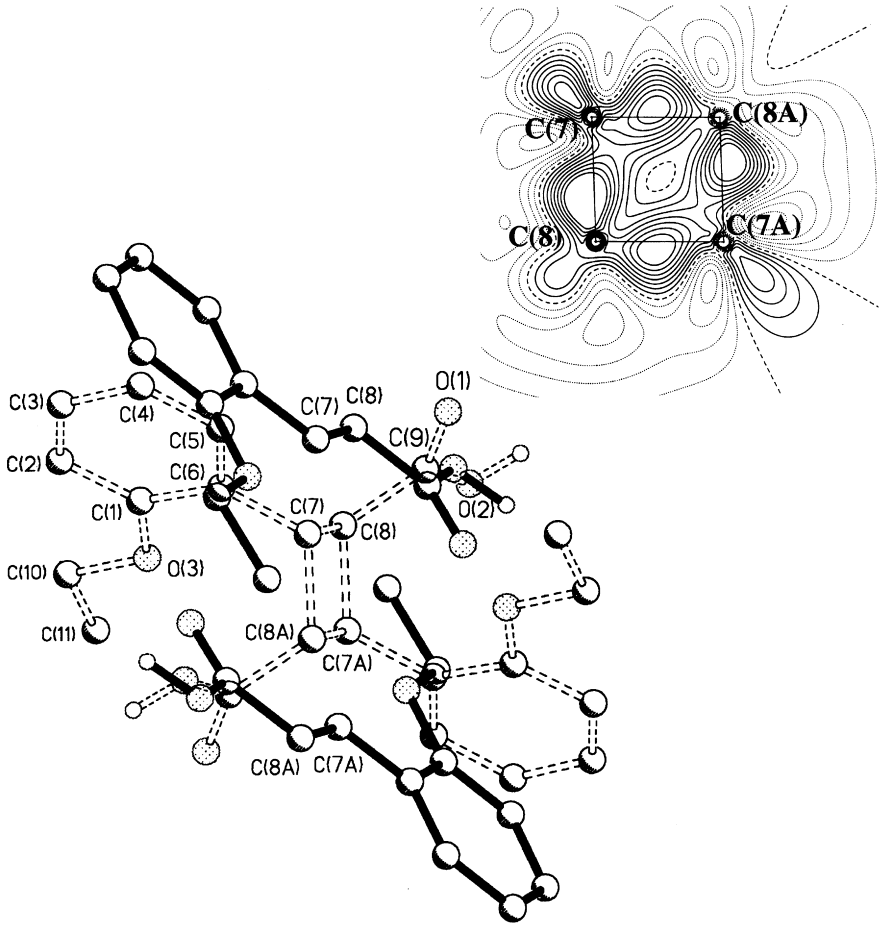

Fig. 8. Photodimerization in *o*-ethoxy cinnamic acid: Two centrosymmetric molecules of the α-form before (full lines) and after (dashed lines) the reaction. Hydrogen atoms other than the hydroxyl are omitted for the sake of clarity. The cinnamoyl double bonds are spaced at ~4.3 Å and following the cycloaddition, a new pair of bonds is formed which are slightly longer (~1.57 Å) than typical C–C bonds. The inset shows the deformation density (at 0.075 eÅ^{-3}) in the plane of the cyclobutane ring in the α-dimer.

motions of all atoms anisotropically. The molecule in the pristine form (Fig. 6a) which is expected to have a two-fold symmetry like naphthalene is unsymmetrical, the asymmetry being reflected only as a small difference in the Laplacian between the two rings. From Fig. 6c, we see that the shape of the contours of the corresponding regions of the two halves of the molecule are somewhat different. Accordingly, the Laplacian values of the N2–C8 and N1–C1 bonds are −15.9 and −13.3 eÅ^{-5}, respectively, while those of C6–C5 and C4–C3 are −21.2 and −18.7 eÅ^{-5}, respectively. Upon protonation (Fig. 6b), noticeable changes occur in bond lengths in the molecule. The C–C bonds are shortened by ~0.01 Å, while the C–N and $C_{aromatic}$–H bonds are lengthened by 0.04 and 0.02 Å, respectively. The $C_{aliphatic}$–H bonds however, do not change considerably. The atomic charges which are negative on the outer carbons decrease as a result of the migration of charge towards proton. These authors also carried out a ^{13}C NMR study in the solid state to show that the outer carbons are deshielded in the complexed proton sponge compared to the uncomplexed one and obtained useful correlations among ρ, $\nabla^2\rho$ and bond lengths. Another interesting aspect of this study is the curved interaction bond path joining two stacked

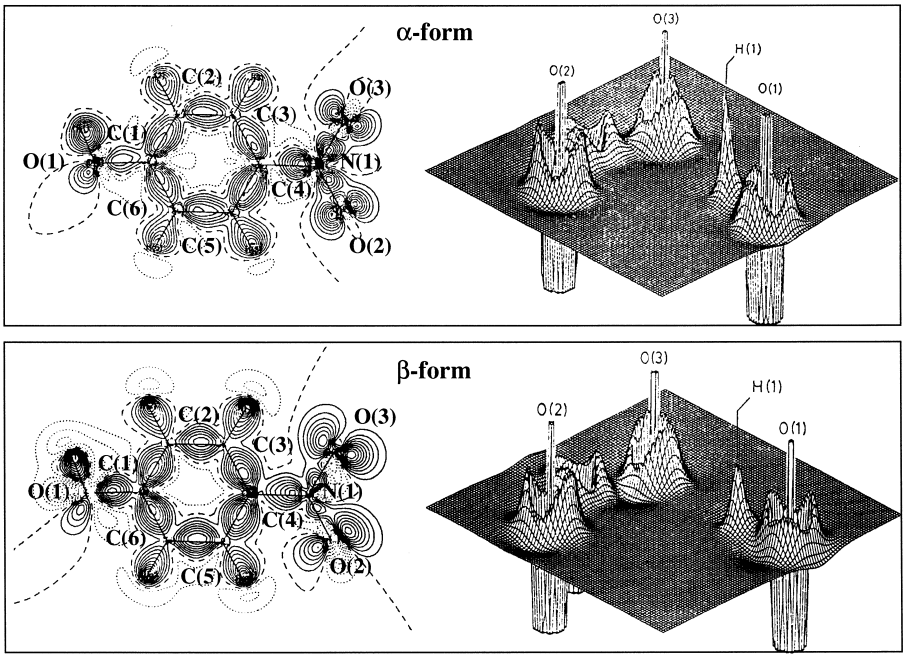

Fig. 9. Polymorphism in *p*-nitrophenol: static deformation density in the plane of the phenyl rings for the α- and the β-forms (contours at 0.1 eÅ^{-3}). Intramolecular and lone-pair regions exhibit many differences. Relief maps of the Laplacians in the intermolecular hydrogen bond region are also shown (range −250 to 250 eÅ^{-5}). In the α-form, H(1) bonds not only with O(3) but also with O(2) and N(1) of the neighboring nitro group (reproduced with permission from Kulkarni et al. [61]).

DMAN molecules attributed to the C–H···π interaction.

Intermolecular hydrogen bonds play a major role in deciding the properties of molecules in the solid state. Cinnamic acids for example, crystallize in two or three polymorphic forms [58], some being photoreactive forming cycloadditives while one polymorph may be photostable. We have carried out a charge density study using a CCD detector on the α- and γ-forms of *o*-ethoxy cinnamic acid (Fig. 7) obtained, respectively, from an ethyl acetate solution and slow cooling of an aqueous ethanol solution [59]. In the reactive α-form, the molecule is found to be quite planar, while in the photostable γ-form, the ethoxy and the cinnamoyl groups make angles of 6.5 and 3.5°, respectively, with the phenyl ring. Interestingly, the latter exhibits near-symmetric hydrogen bonds in the intermolecular region. The hydrogen H(2A) was located midway between the oxygens with the O–H and H···O distances of 1.23 and 1.39 Å, respectively. Accordingly, the ρ_{CP} values associated with the two bonds are comparable, ∼1.6 and 0.8 eÅ^{-3}, respectively. Moreover, the intermolecular bond carries a negative Laplacian (∼ − 12.4 eÅ^{-5}) like a hydroxy bond which is indicative of a highly shared interaction. In the α-form, on the other hand, the O–H and H···O distances are usual (0.96 and 1.68 Å, respectively) with ρ_{CP} of 2.2 and 0.32 eÅ^{-3}, respectively. The H(2A)···O(1) hydrogen bond shows a small positive Laplacian of 4.81 eÅ^{-5} as is generally expected for a closed shell interaction. The other interesting aspect of this study is the inference on delocalization of the π-density in the α-molecule, from the cinnamoyl double bonds to the neighboring single bonds and across the phenyl group. This is also in compliance with the molecule being planar in this polymorph. A complete absence of such an effect in the γ-form was interpreted as due to the ionic nature induced by the symmetric hydrogen bonds. These factors influence the molecular geometry and the packing which in turn decide reactivity of a polymorphic form. The cinnamoyl bond undergoes (2 + 2) cycloaddition in the α-polymorph. Structural analysis indicated favorable approach of the

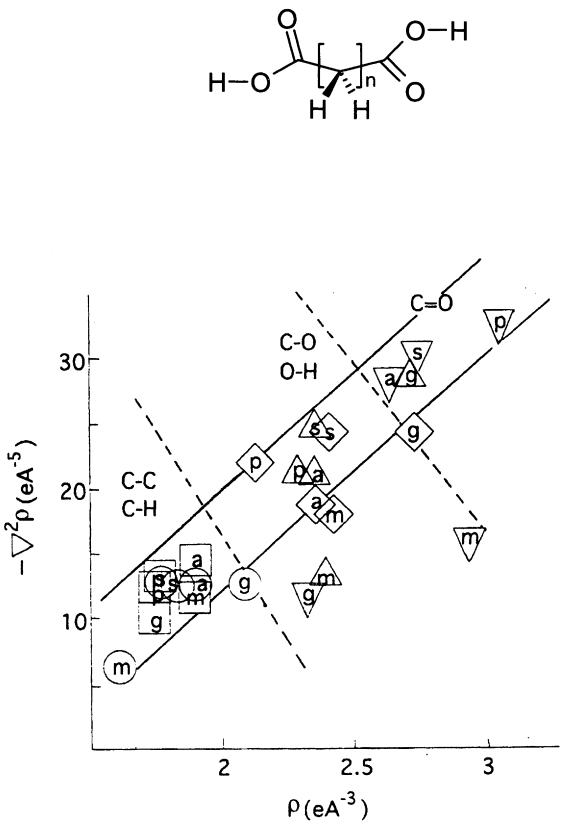

Fig. 10. Alkanedioic acids: variation of Laplacian with charge density at the critical point for various bonds, C–C, circle; C–H, square; C–O, up-triangle; C=O, down-triangle and O–H, rhombus. The letters m, s, g, a and p marked inside the data symbols represent bonds belonging to malonic, succinic, glutaric, adipic and pimelic acids, respectively. The different bond regions are delineated (reproduced with permission from Gopalan et al. [63]).

centrosymmetrically related cinnamoyl bonds in the photoactive α-form (Fig. 8). The deformation density of the cyclobutyl ring resulting from the photodimerization of α-form is shown in the inset of Fig. 8. It exhibits a (3, +1) CP at the inversion center of the ring associated with small density (0.62 eÅ^{-3}) and Laplacian (6.6 eÅ^{-5}). The densities of the ring bonds are small (∼1.51 eÅ^{-3}) implying that the bonds are weak. They are also associated with high ellipticity (∼0.2) and polarization (6%). The contours of these bonds lie outside the interatomic vector, the vertical displacement being ∼0.04 Å, characteristic of bent bonds in a strained ring [17,45].

p-Nitrophenol is known to show interesting photochemical activity only in one of its polymorphic forms. The α-form which crystallizes from benzene undergoes a topochemical transformation up on irradiation, changing its color from yellow to red, though structural changes associated with the transformation have been found to be insignificant [60]. On the other hand, the β-form obtained from aqueous solution, is light-stable. This has been the subject of a charge density study [61] (Fig. 9). It is found that the phenyl ring bonds in the α-form exhibit less density (∼2.05 eÅ^{-3}) compared to those in the β-form (∼2.21 eÅ^{-3}) as though charge had migrated outwardly in the former. Accordingly, the nitro and the hydroxyl bonds in the latter were found to carry relatively higher densities. The authors found many differences in the hydrogen bonding as well. In the β-form, there are four hydrogen bonds compared to six in the α-form. The striking difference between the two polymorphs is that in the α-form, the entire nitro group participates in hydrogen bonding with the neighboring hydroxyl hydrogen while in the β-form only the nitro oxygens involve in the hydrogen bonding. Interestingly upon photoirradiation of the α-form, charge density redistribution seems to occur with the reacted product assuming an intramolecular density similar to that found in the light stable β-form [62]. The authors have estimated the molecular dipole moments to be 18.0 and 21.5 Debye for the α- and β-forms, respectively and a somewhat lower moment in the case of the irradiated α-form, ∼9.9 Debye.

The lattice cohesion of the first few members of the homologous series of aliphatic dicarboxylic acids has been investigated in terms of charge density [63]. These acids form an interesting class of organic compounds in that the structure and properties in the solid state exhibit undulatory behavior with the number of methylene groups being odd or even [64]. For example, the melting point alternates in the series malonic, succinic, glutaric, adipic, pimelic and so on. The study yielded interesting systematics in the charge densities and the Laplacians along the series. The ρ_{CP} values of C–C, C–O and O–H bonds increase from malonic (1.61, 2.27 and 2.45 eÅ^{-3}, respectively) to glutaric (2.18, 2.72 and 2.7 eÅ^{-3}, respectively) and decrease thereafter. The C=O and C–H bonds exhibit the opposite trend with glutaric acid carrying the minimum charge density ∼2.33 and 1.66 eÅ^{-3}, respectively. An overall

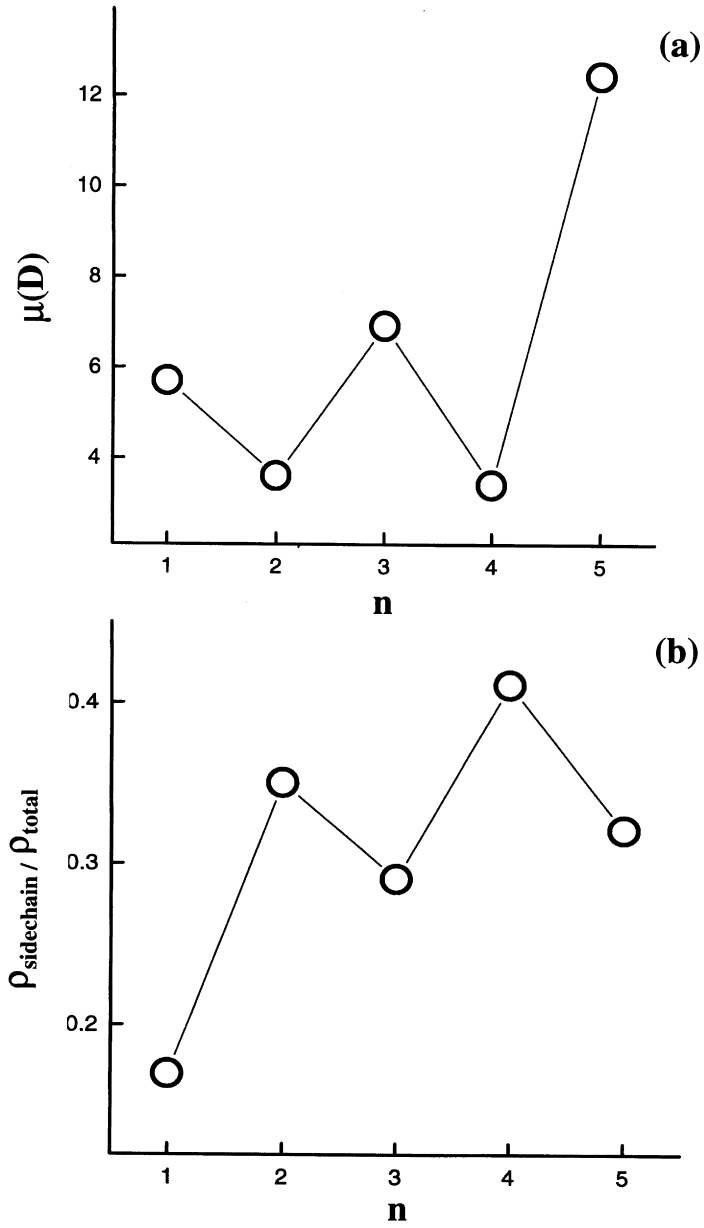

Fig. 11. (a) Molecular dipole moments of the dicarboxylic acids. Values obtained for the asymmetric units are shown since net dipole moment for an even acid vanishes due to center of symmetry. Here, *n* denotes the number of methylene groups in the acid. (b) A plot of the sum of ρ_{CP} obtained for the side-chain interactions normalized with the total ρ_{CP} due to intermolecular interactions, against the number of methylene groups, *n*, in the acid (reproduced with permission from Gopalan et al. [63]).

assessment of the charge distribution among various bonds can be made by plotting the Laplacian against the density for various bonds as shown in Fig. 10. We see that most bonds lie in a region where the Laplacian is roughly proportional to the bond density, as one would normally expect. Thus, the C–C and the C–H bonds fall in the first region of the plot while the C–O and the O–H bonds group fall in the second

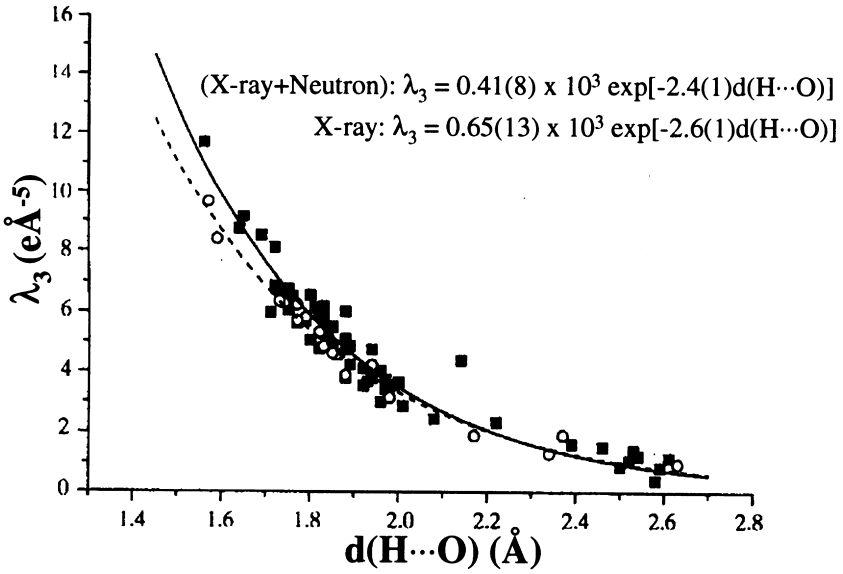

Fig. 12. Variation of the positive curvature, λ_3 at bond CP, with hydrogen contact distance, d(H···O). The data points obtained from a number of charge density investigations reported in the literature and were fitted using exponential equations. Circles and dashed line; joint X-ray and neutron, filled squares and solid line; X-ray data only. Among the three eigenvalues, λ_3 was found to be giving the best representation for hydrogen bonds having closed-shell interactions (reproduced with permission from Espinosa et al. [65]).

region. The C=O bonds are found in the third region. The C–O and C=O bonds of the malonic and the glutaric acids are somewhat unusual. In the case of the malonic acid, the Laplacians of the two bonds are noticeably lower. In glutaric acid, on the other hand, the Laplacian of the C=O bond is lower than that of the C–O bond, a trend which is reflected in the charge densities as well.

An important outcome of the study of the dicarboxylic acids is the analysis of the dipole moments of the asymmetric units in relation to intermolecular interactions in the crystal lattice (Fig. 11a). It is interesting that the dipole moments showed alternation along the series with the odd acids having higher moments than the even neighbors with pimelic acid exhibiting the highest moment, 12.7 Debye. The strength of molecular packing in the lattice was guided by the value of the sum of the ρ_{CP}s associated with side chain C–H···O interactions expressed as a fraction of the total intermolecular density due to C–H···O and O–H···O interactions (Fig. 11b). Interestingly, there is an alternation in this value along the series with the even acids exhibiting higher values compared to their odd neighbors. Thus, it appears that increased side-chain interactions in the even acids lead to distributed bond dipoles thereby decreasing the net dipole moment in the asymmetric unit. This may also be the reason for the relatively higher melting points in the even acids, since side-chain interactions as compared to the dimeric bonds play a decisive role in the cohesion of acid molecules in the solid state.

Hydrogen bonds have been classified by many workers in terms of varying degrees of shared and closed-shell interactions. Correlations between $\nabla^2\rho$ and ρ, as shown above in Fig. 10 find good agreement only within a group of like-hydrogen bonds. A more general approach has been suggested by Espinosa et al. [65] who used the variation of positive curvature along the interaction axis (λ_3) at CP with the hydrogen bond distance and obtained a well-defined behavior as shown in Fig. 12. The value of λ_3 was found to increase exponentially with decreasing hydrogen bond distances. It represents the overlap between the electron cloud of both H and O atoms at the critical point and is proportional to the kinetic energy density, G_{CP}.

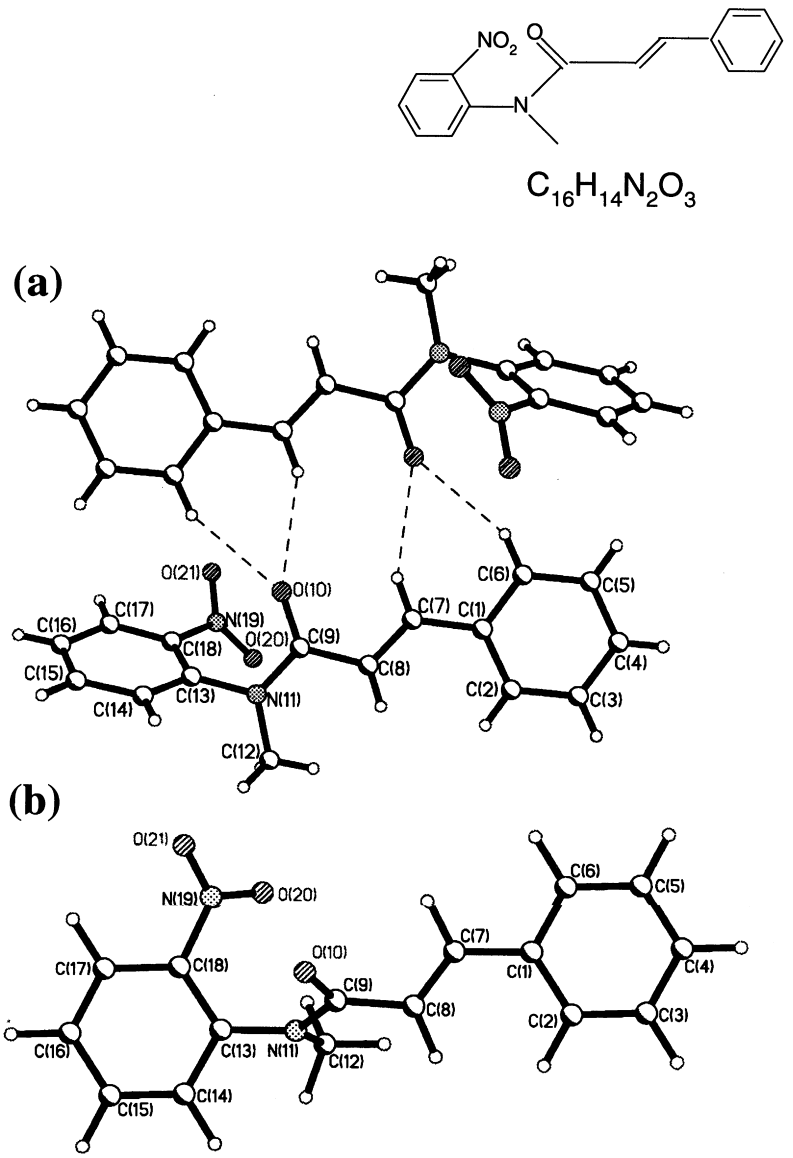

Fig. 13. Molecular structure of *N*-methyl-*N*-(2-nitrophenyl)cinnamanilide from (a) X-ray crystallography (bifurcated intermolecular hydrogen bonds are also shown) (b) AM1 calculation. Formula diagram is given in the inset (reproduced with permission from Gopalan et al. [68]).

8. Molecular packing in crystals

The geometry of a molecule in the solid state may deviate significantly from that in the free state, an effect which is mainly due to the constraints of packing in a lattice. For instance, the nitrobenzene molecule which is known to be planar in the free state is twisted by about 2° in the solid state across the nitro–benzene link. On the contrary, biphenyl [66] is non-planar in both gaseous and liquid states while it is planar [67] in the crystal at room temperature, exhibiting D_{2h} symmetry compared to D_2 in the former. Polymorphism in molecular crystals discussed above, is another subject of interest in this context. It is considered to be important to understand the symmetries prevailing in a molecular solid in terms of

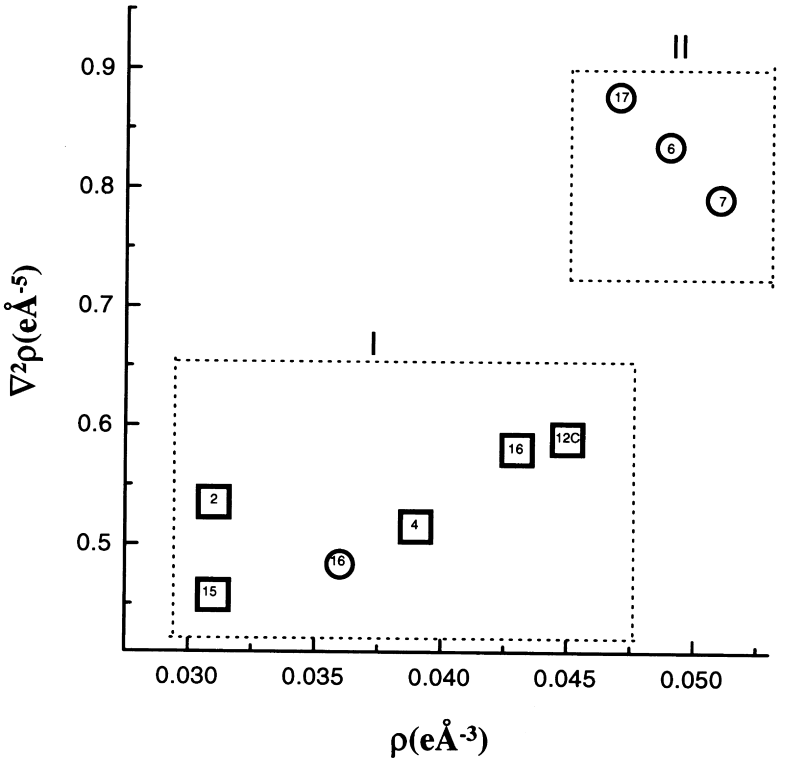

Fig. 14. Variation of the Laplacian with density at the critical points for various hydrogen bonds, $O_{amido}\cdots H$, circles; $O_{nitro}\cdots H$, squares. The numbers inside the symbols refer to the hydrogens involved in bonding. Regions I and II emphasize different trends in the plot (reproduced with permission from Gopalan et al. [68]).

the distortions of the molecules and the nature of the intermolecular interactions.

Gopalan et al. [68] have carried out a charge density investigation on *N*-methyl-*N*-(2-nitrophenyl)cinnamanilide. The molecule exhibits a highly favored bifurcated C–H···O hydrogen bond ring structure in the lattice and is also considerably distorted (Fig. 13a). It is twisted at the amide-phenyl link with the cinnamide portion being nearly planar (torsion angle, C(2)–C(1)–C(7)–C(8), −6.24°). The nitrobenzene ring is highly non-planar, the nitro group being rotated with respect to the phenyl ring by ∼43.5°. The nitrobenzene group as a whole is twisted away from the mean cinnamide plane making an angle of 63.3°. The molecular structure in the lattice as discussed above was compared with that of a free molecule shown in Fig. 13b. The latter was obtained using AM1-PRECISE calculation of MOPAC [38] after optimizing the bond lengths, angles and torsion angles. The experimental coordinates served as the initial input. An important finding from the calculation is that the benzene rings are parallel within 8° while the intervening bonds are buckled with high torsion angles (see Fig. 13b). This calculation provides a reference state of the molecule using which constraints imposed by packing in a lattice could be examined.

Several intermolecular hydrogen bond contacts were examined. Four C–H···O contacts were found to originate from the amidic oxygen (two involved in bifurcated bond) while six from the nitro-oxygens. The results of the charge density analysis is shown in Fig. 14. The $\nabla^2\rho-\rho$ plot consists of two regions of interactions as shown—one region, where the hydrogen bonds exhibit low values of both the density and the Laplacian and the other, where both quantities are disproportionately higher. What is interesting is that all the bonds involving the nitro-oxygens belong to the first region and those from the amidic oxygen

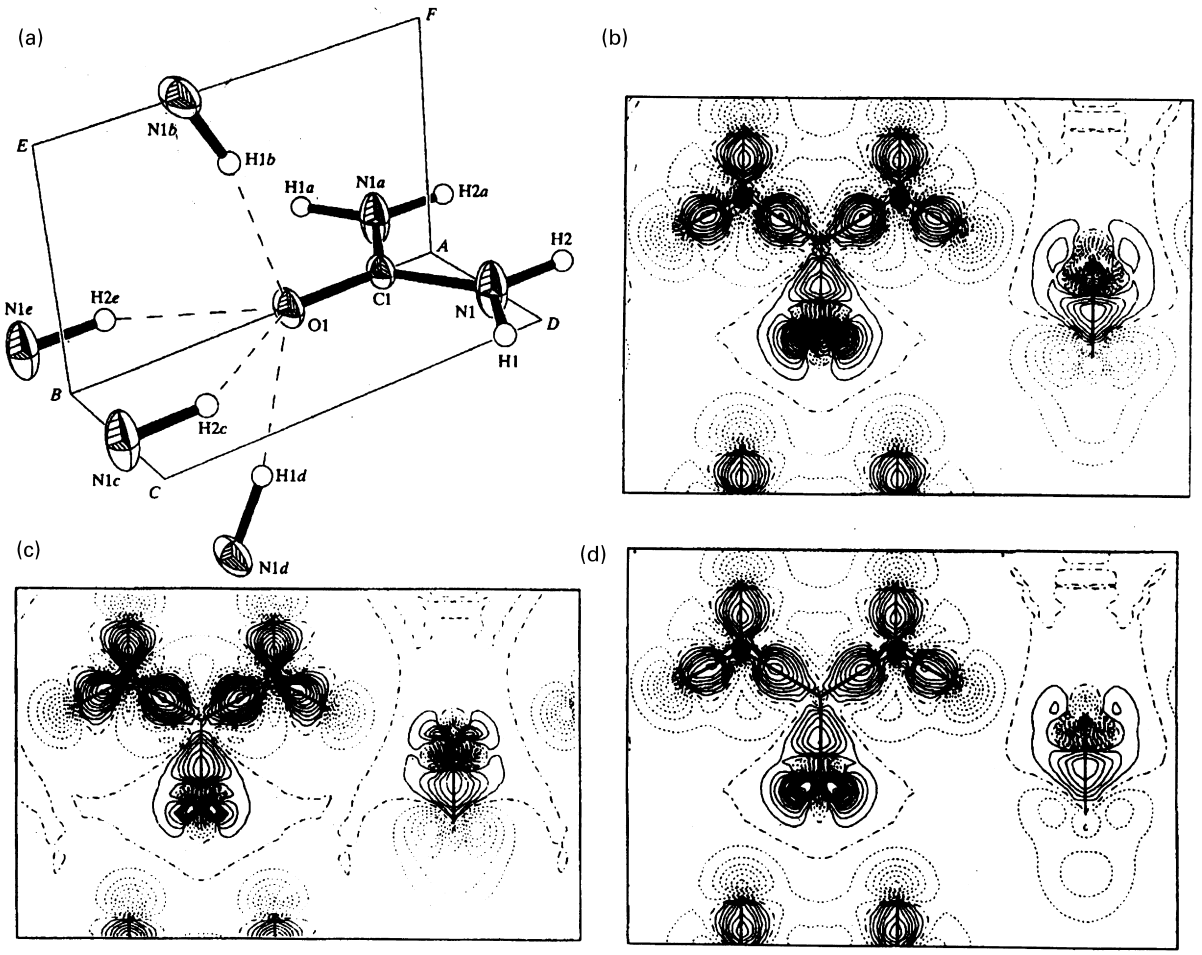

Fig. 15. (a) Intermolecular hydrogen bonds in urea crystal with displacement ellipsoids at 50% probability. (b) Static deformation density obtained from the multipolar analysis of the experimental data corrected for the thermal diffuse scattering. Theoretical deformation density obtained using (c) the Hartree–Fock method; (d) the DFT method by generalized gradient approximation (contours at 0.0675 eÅ^{-3}) (reproduced with permission from Zavodnik et al. [69]).

fill the second region. Clearly, the amidic oxygen forms stronger hydrogen bonds compared to the more ionic nitro-oxygens. It is as though to favor bifurcated hydrogen bonding from the amidic oxygen, the molecule is highly twisted at the amide–nitrobenzene link.

Urea, despite being simple and highly symmetric (C_2), is known to crystallize in a non-centric crystal system (P-42$_1m$). The molecules are linked to each other through hydrogen bonds forming infinite tapes, adjacent tapes being held by orthogonal hydrogen bonds. This is perhaps the only example containing a carbonyl group involved in four hydrogen bonds (Fig. 15a). Feil and co-workers [69] performed X-ray diffraction at 148 K and carried out charge density analysis on the data corrected for thermal diffuse scattering. They have also done orbital calculations in lattice using CRYSTAL95 [39] by both Hartee–Fock and DFT methods, the latter in both local density and generalized gradient approximations. The authors compared deformation densities and structure factors obtained from the experimental charge density analysis with those obtained from theoretical procedures. The deformation density maps from experiment and

theory (compare Fig. 15b–d) were found to be in good agreement. The density functional theory seemed to yield slightly better results compared to the Hartree–Fock calculations.

Gatti et al. [70] have described the unusual hydrogen bonding in urea based on computations. They considered three cases of the urea molecule. A molecule as in the bulk structure with inputs from neutron diffraction, was computed using CRYSTAL92 [39] with 6-31 G** basis sets. In the second case, the free molecule was held at the crystal geometry and in the third, at more optimized geometry with only the C_{2v} constraint. Geometry optimization were done using GAUSSIAN92 with spherical harmonic gaussian functions. Compared to the free molecule, they found that the heavy atoms of the molecule in the bulk gain electrons at the expense of the hydrogens, the flux being $\sim 0.06e$. The fields created by such charge transfer polarizes the molecule in the bulk enhancing dipole moments. They observed that the ellipticity and ρ increase for the C–N bonds on passing from gas to bulk while for all the other bonds, both ellipticity and ρ decrease. These changes were found to comply with strengthening of the C–N bonds in terms of increased covalency and π-character. Other bonds in the molecule become more ionic on passing from gas to bulk. The ellipticity associated with the intermolecular hydrogen bonds along infinite planar tapes was found to be similar to that in the π-plane of the molecule. Based on this, the authors have argued that the π-conjugation propagates through these hydrogen bonds.

The above study has also shown that the carbonyl oxygen actually forms an active center for hydrogen bonding. The oxygen lone-pairs being electron-rich regions in the base, are characterized by high negative Laplacians in the free molecule (145.82 eÅ^{-5}) while those associated with nitrogen carry much smaller Laplacians (54.85 eÅ^{-5}). In the bulk, when oxygens get involved in hydrogen bonding, the lone-pair Laplacians were found to decrease to $\sim$136.62 eÅ^{-5}. The two saddle points in between the lone-pairs which lie above and below the molecular plane are the second most electron-rich regions (89.26 eÅ^{-5}) which are seen as maxima by hydrogens approaching perpendicularly. Accordingly, the Laplacian associated with the saddle point increases to 94.3 eÅ^{-5} in the bulk. The valence shell charge concentration of oxygen therefore changes in such a way so as to form a torus of nearly uniform charge concentration in the non-bonded region. The authors conclude that the lengthening of the C=O bond in bulk urea by 0.13 Å accompanied by decreasing ellipticity and associated changes in the oxygen non-bonded regions is a fundamental step for the creation of a three-dimensional network of hydrogen bonds. This may be a more general mechanism in the formation of hydrogen bonded molecular crystals as was shown in the case of the cinnamanilide molecule.

9. Molecular NLO materials

In the last few years, several workers have analyzed charge density distribution in molecular crystals with non-linear optical (NLO) properties [71–74]. The NLO response can, in principle, be explained by an anharmonic distortion of the electron density distribution due to the electric field of an applied optical pulse. The polarization P induced in a molecule is

$$P = \mu + \alpha E + \beta E^2 + \cdots \tag{16}$$

where μ is the ground state dipole moment and α and β are the linear and the quadratic polarizabilities of the molecules, respectively. However, determination of polarizability from X-ray diffraction requires careful handling of data. Many of the studies on NLO crystals using charge density concentrate merely on the accurate extraction of phases associated with the structure factors [75–78],

$$\Delta\rho(\mathbf{r}) = V^{-1} \sum_{\mathbf{h}} [|F_{\mathrm{m}}(\mathbf{h})| \exp \mathrm{i}\varphi_{\mathrm{m}}(\mathbf{h}) - |F_{\mathrm{s}}(\mathbf{h})| \exp \mathrm{i}\varphi_{\mathrm{s}}(\mathbf{h})] \exp(-2\pi \mathrm{i}\mathbf{hr}) \tag{17}$$

where the subscripts m designate the atom-centered multipolar density model, and s, the spherically averaged free-atom superposition model. The deformation density therefore, can be written as the sum of an amplitude deformation density and a phase deformation density,

$$\Delta\rho = \Delta\rho(\Delta|F|) + \Delta\rho(\Delta\varphi) \tag{18}$$

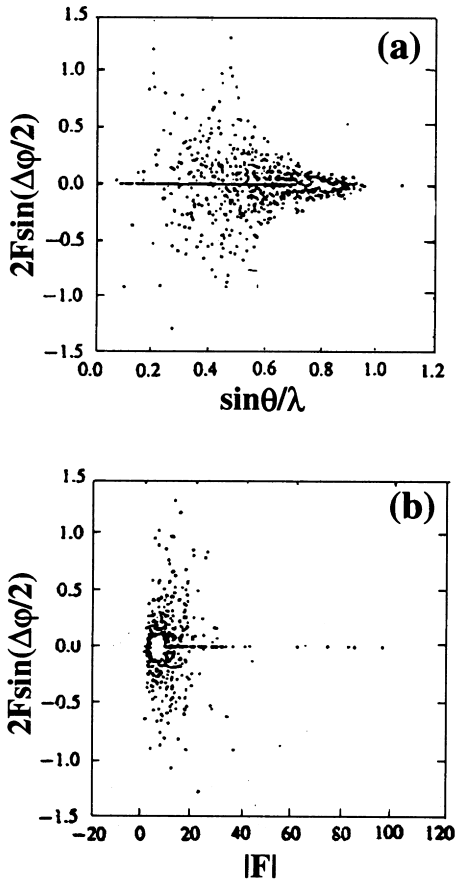

Fig. 16. Distribution of $2F\sin(\Delta\varphi/2)$ against (a) $(\sin\theta/\lambda$; and (b) $|F|$ (reproduced with permission from Hamazaoui et al. [76]).

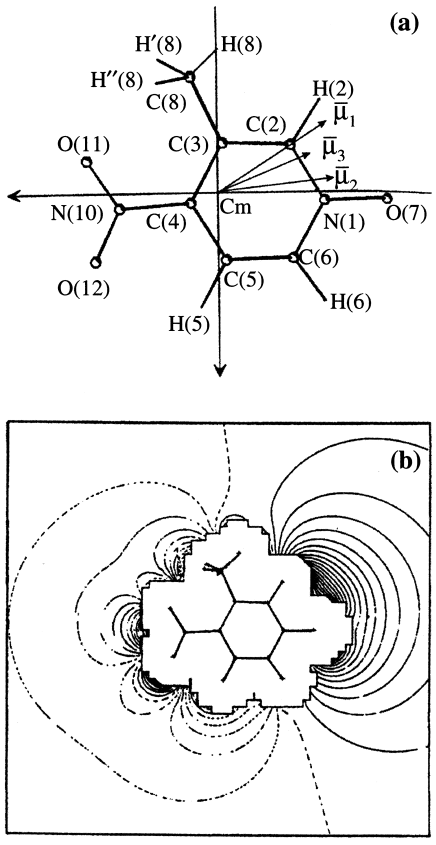

Fig. 17. (a) Orientation of molecular dipole moments in 3-methyl-4-nitropyridine *N*-oxide: μ_1, molecular dipole moment from direct integration methods; μ_2, from multipolar model; and μ_3 from semi-empirical calculation. (b) Electrostatic potential around the molecule in the plane of ring atoms. Contours at 0.2 kcal/mol (reproduced with permission from Hamazaoui et al. [79]).

where

$$\Delta\rho(\Delta|F|) = V^{-1}\sum(|F_m| - |F_s|)\exp(i\varphi_m) \times \exp(-2\pi i\mathbf{hr}) \quad (19)$$

and

$$\Delta\rho(\Delta\varphi) = V^{-1}\sum 2|F_s|\sin(\Delta\varphi/2)\exp[i(\varphi_s + \varphi_m + \pi)/2]\exp(-2\pi i\mathbf{hr}) \quad (20)$$

For a given data set, it is instructive to examine the magnitude of $2F\sin(\Delta\varphi/2)$ in order to understand the effect of phase correction on the final solution. Fig. 16 shows the distribution of $2F\sin(\Delta\varphi/2)$ as a function of $\sin\theta/\lambda$ and $|F|$, from a data set due to Hamazaoui et al. [76]. It is apparent that the magnitude of phase correction is relatively higher for the low-order reflections (<0.6 Å^{-1}) as well as for weak- and medium-intensity reflections. Consequently, the measurement and the processing of the low angle weak reflections deserve special care. The authors have also shown that the overall charge density increases by ~25% after phase correction. Besides phase correction, the authors carried out thermal analysis involving rigid bond tests. Such corrections are highly recommendable while determining charge density in non-centric crystals.

There has been some attempt to calculate of

hyperpolarizability from higher moments, but a more acceptable quantitative connection is yet to be established. Fkyerat et al. using octupole moments of the charge distribution in *N*-(4-nitrophenyl)-L-prolinol [73,74] estimated β to be 42.9 $e\text{Å}^{-3}$ and compared with the experimental result $\sim$39.14 $e\text{Å}^{-3}$. They concluded that NPP is a one-dimensional non-linear compound with β oriented almost along the main axis of the molecule making only 19.8° with the dipole moment vector.

Other studies on NLO crystals report topological analysis of deformation density and electrostatic potential and also on the calculation of molecular dipole moment. Hamazaoui et al. have carried out an experimental charge density study on 3-methyl-4-nitro-pyridine-*N*-oxide [79] and have computed the molecular dipole moments by three different procedures namely semi-empirical calculation, multipolar model and direct integration method. In all the methods, the dipole moment points nearly towards *N*-oxide group as shown in Fig. 17a. They found a close agreement between the semi-empirical and multipolar models while that from direct integration differed considerably in the direction of the dipole moment. The authors attributed this difference to the deconvolutability of thermal parameters from electron density in the case of multipolar refinement which is not possible in direct integration. The dipole moment of this molecule (1 Debye) was compared with that of nitropyridine *N*-oxide, a closely related molecule in which the methyl group in the *meta*-position is absent. The latter was found to have a much smaller dipole moment (0.4 Debye) [80]. On this basis, the authors concluded that the introduction of a methyl group in the *meta*-position favors intramolecular charge transfer. They have also determined the electrostatic potential in the plane of the ring which showed positive electrostatic potential around the *N*-oxide group and a negative electrostatic potential around the nitro group (Fig. 17b) thereby confirming the nature of charge transfer as found by the orientation of the molecular dipole moment.

10. Conclusions

In this article, we have dealt with the salient features of the electronic charge density distribution in molecular solids obtained by both theory and experiment. The importance of comparative experimental and theoretical studies of electron density is pointed out. The topological analysis of the density is illustrated taking representative examples. The chemical aspects of the charge distribution is described in terms of the deformation density, the Laplacian of the total density as well as the electrostatic potential. The polarization of the electron density in cyano bonds of diisocyanomethane, π/π' delocalization in the phosphazene ring and the bent cage bonds in cubane are some of the examples discussed. In addition, cases revealing the interplay between the intermolecular hydrogen bonding and properties are examined. These include proton sponges, polymorphic forms of cinnamic acid and *p*-nitrophenol where one of the forms exhibits photochemical reactivity. The role of intermolecular hydrogen bonding in lattice cohesion is discussed for a series of dicarboxylic acids. Molecular distortions in urea and cinnamanilide molecules are explained on the basis of the strength of the surrounding hydrogen bonds. Molecules exhibiting NLO properties in the solid state such as *N*-(4-nitrophenyl)-L-prolinol have been discussed, focusing on the intramolecular charge transfer leading to enhanced dipole moments.

References

[1] P. Debye, Dispersion of Roentgen rays, Ann. Phys. 46 (1915) 809.
[2] R.F.W. Bader, Atoms in Molecules—A Quantum Theory, Clanderon Press, Oxford, 1990.
[3] P. Coppens, Annu. Rev. Phys. Chem. 43 (1992) 663.
[4] D. Feil, J. Mol. Struct. 255 (1992) 221.
[5] F.L. Hirshfeld, in: A. Domenicano, I. Hargittai (Eds.), Accurate Molecular Structures. Their Determination and Importance, IUCr/Oxford University Press, Oxford, 1992, p. 237.
[6] F.L. Hirshfeld, Crystallogr. Rev. 2 (1991) 169.
[7] M.A. Spackman, Chem. Rev. 92 (1992) 1769.
[8] V.G. Tsirelson, R.P. Ozerov, J. Mol. Struct. 255 (1992) 335.
[9] G.A. Jeffrey, J.F. Piniella (Eds.), The Application of Charge Density Research to Chemistry and Drug Design Plenum Press, New York, 1991.
[10] P. Coppens, X-ray Charge Densities and Chemical Bonding, Oxford University Press, Oxford, 1997.
[11] R. Blessing (Ed.), Studies of electron distributions in molecules and crystals, Trans. Am. Crystallogr. Assoc., 26 (1990).
[12] T. Koritsanszky, in: W. Gans, A. Amann, J.C.A. Boeyens (Eds.), Fundamental Principles of Molecular Modelling, Plenum Press, New York, 1996, p. 143.

[13] M.A. Spackman, A.S. Brown, Annu. Rep. Prog. Chem. Sect. C: Phys. Chem. 91 (1994) 175.
[14] M.A. Spackman, Annu. Rep. Prog. Chem. Sect. C: Phys. Chem. 94 (1998) 177.
[15] P. Coppens, Acta Crystallogr. A54 (1998) 779.
[16] N.K. Hansen, P. Coppens, Acta Crystallogr. A34 (1978) 909.
[17] D. Cremer, E. Kraka, Croat. Chem. Acta 57 (1984) 1259.
[18] P. Politzer, D.G. Truhlar (Eds.), Chemical Applications of Atomic and Molecular Electrostatic Potentials Plenum Press, New York, 1981.
[19] J.S. Murray, K.D. Sen (Eds.), Molecular Electrostatic Potentials: Concepts and Applications Elsevier, Amsterdam, 1996.
[20] Y. Abramov, Acta Crystallogr. A53 (1997) 264.
[21] P. Coppens, Y. Abramov, M. Carducci, B. Korjov, I. Novozhilova, C. Alhambra, M.R. Pressprich, J. Am. Chem. Soc. 121 (1999) 2585.
[22] E. Espinosa, E. Mollins, C. Lecomte, Chem. Phys. Lett. 285 (1998) 170.
[23] P. Macchi, D.M. Prosperpio, A. Sironi, R. Soave, R. Destro, J. Appl. Crystallogr. 31 (1998) 583.
[24] A. Volkov, G. Wu, P. Coppens, J. Synchroton. Rad. 6 (1997) 1007.
[25] T. Koritsansky, R. Flaig, D. Zobel, H.-G. Crane, W. Morgenroth, P. Luger, Science 279 (1998) 356.
[26] G.M. Sheldrick, SHELX-76, Program for crystal structure determination, University of Göttingen, Germany.
[27] F.H. Allen, O. Kennard, D.G. Watson, L. Brammer, A.G. Orpen, R. Taylor, J. Chem. Soc. Perkin Trans. II (1987) S1.
[28] F.L. Hirshfeld, Acta Crystallogr. A32 (1976) 239.
[29] V. Schoemaker, K.N. Trueblood, Acta Cryst. B54 (1998) 507.
[30] T. Koritsansky, S.T. Howard, T. Richter, P.R. Mallinson, Z. Su, N.K. Hansen, XD, A computer program package for multipole refinement and analysis of charge densities from diffraction data, Cardiff, Glasgow, Buffalo, Nancy, Berlin.
[31] R.F. Stewart, M.A. Spackman, VALRAY User's Manual, Carnegie Mellon University, Pittsburgh, PA.
[32] H.L. Hirshfeld, Acta Crystallogr. A32 (1976) 239.
[33] B.M. Craven, H.P. Weber, X. He, Technical Report TR-87-2, Department of Crystallography, University of Pittsburgh, PA, 15260, 1987.
[34] W.J. Hehre, L. Radom, P.v.R. Schleyer, J.A. Pople, Ab initio Molecular Orbital Theory, Wiley, New York, 1986.
[35] J.A. Pople, Angew. Chem. Int. Ed. Engl. 38 (1999) 1894.
[36] M.J. Frisch, G.W. Trucks, H.B. Schlegel, P.M.W. Wong, J.B. Foresman, M.A. Robb, M. Head-Gordon, E.S. Replogle, R. Gomperts, J.L. Andres, K. Raghavachari, J.S. Binkley, C. Gonzalez, R.L. Martin, D.J. Fox, D.J. Defrees, J. Baker, J.J.P. Stewart, J.A. Pople, GAUSSIAN 92/DFT, Revision G.4, Gaussian Inc., Pittsburgh, PA, 1993.
[37] M.W. Schmidt, K.K. Baldridge, J.A. Boatz, S.T. Elbert, M.S. Gordon, J.H. Jensen, S. Koseki, N. Matsunaga, K.A. Nguyen, S.J. Su, T.L. Windus, M. Dupuis, J.A. Montgomery, Gamess, J. Comput. Chem. 14 (1993) 1347.
[38] J.J.P. Stewart, J. Comput.-Aided Mol. Des. 4 (1990) 1.
[39] R. Dovesi, V.R. Saunders, C. Roetti, M. Causa, N.M. Harrison, R. Orlando, R. Apra, CRYSTAL95 User's Manual, University of Turin, Turin, Italy, 1996.
[40] T. Koritsanszky, J. Buschmann, D. Lentz, P. Luger, G. Peretuo, M. Rottger, Chem. Eur. J. 5 (1999) 3413.
[41] M.J.S. Dewar, E.A.C. Lucken, M.A. Whitehead, J. Chem. Soc. (1960) 243.
[42] D.P. Craig, N.L. Paddock, J. Chem. Soc. (1962) 4118.
[43] T.S. Cameron, B. Boreka, W. Kwiatkowski, J. Am. Chem. Soc. 116 (1994) 1211.
[44] H. Irngartinger, A. Wesler, T. Oeser, Angew. Chem. Int. Ed. Engl. 38 (1999) 1279.
[45] H. Irngartinger, S. Strack, J. Am. Chem. Soc. 120 (1998) 5818.
[46] K.B. Wilberg, C.M. Hadad, C.M. Breneman, K.E. Laidig, M.A. Murcko, T.J. LePage, Science 252 (1991) 1266.
[47] I. Alkorta, J. Elguero, C. Foces-Foces, Chem. Commun. (1996) 1633.
[48] I. Rozas, I. Alkorta, J. Elguero, J. Phys. Chem. A 102 (1998) 9925.
[49] I. Rozas, I. Alkorta, J. Elguero, J. Phys. Chem. A 101 (1997) 9457.
[50] I. Rozas, I. Alkorta, J. Elguero, J. Phys. Chem. A 101 (1997) 4236.
[51] I. Alkorta, J. Elguero, J. Phys. Chem. (1996) 100.
[52] Y.H. Zhang, J.-K. Hao, X. Wang, W. Zhou, T.-H. Tang, J. Mol. Struct. (Theochem) 455 (1998) 85.
[53] D. Madsen, C. Flensburg, S. Larsen, J. Phys. Chem. A 102 (1998) 2177.
[54] G.K.H. Madsen, B.B. Iversen, F.K. Larsen, M. Kapon, G.M. Reisner, F.H. Herbstein, J. Am. Chem. Soc 120 (1998) 10040.
[55] Y.A. Abramov, L. Brammer, W.T. Klooster, R.M. Bullock, Inorg. Chem. 37 (1998) 6317.
[56] P.R. Mallinson, K. Wozniak, T. Garry, K.L. McCormak, J. Am. Chem. Soc. 119 (1997) 11502.
[57] P.R. Mallinson, K. Wozniak, C.C. Wilson, K.L. McCormak, D.M. Yufit, J. Am. Chem. Soc. 121 (1999) 4640.
[58] M.D. Cohen, G.M.J. Schmidt, F.I. Sonntag, J. Chem. Soc. (1964) 2000.
[59] R.S. Gopalan, G.U. Kulkarni, C.N.R. Rao, Acta Cryst. B (2000) in press.
[60] P. Coppens, G.M.J. Schmidt, Acta Crystallogr. 17 (1964) 222.
[61] G.U. Kulkarni, P. Kumaradhas, C.N.R. Rao, Chem. Mater. 10 (1998) 3498.
[62] P. Kumaradhas, R.S. Gopalan, G.U. Kulkarni, Proc. Indian Acad. Sci. (Chem. Sci.) 111 (1999) 569.
[63] R.S. Gopalan, P. Kumaradhas, G.U. Kulkarni, C.N.R. Rao, J. Mol. Struct. (2000) (in press).
[64] R.T. Morrison, R.N. Boyd, Organic Chemistry, 5th ed., Prentice-Hall, London, 1987 (p. 846).
[65] E. Espinosa, M. Souhassou, H. Lachekar, C. Lecomte, Acta Crystallogr. B55 (1999) 563.
[66] O. Bastiansen, Acta Chem. Scand. 3 (1949) 408.
[67] A. Chakrabarti, S. Yashonath, C.N.R. Rao, Mol. Phys. 84 (1995) 49.
[68] R.S. Gopalan, G.U. Kulkarni, E. Subramanian, S. Renganayaki, J. Mol. Struct. (2000) (in press).
[69] V. Zavodnik, A. Stash, V. Tsirelson, R. De Vries, D. Feil, Acta Crystallogr. B55 (1999) 45.

[70] C. Gatti, V.R. Saunders, C. Roetti, J. Chem. Phys. 101 (1994) 10686.
[71] S.T. Howard, M.B. Hursthouse, C.W. Lehmann, P.R. Mallinson, C.S. Frampton, J. Chem. Phys. 97 (1992) 5616.
[72] E. Espinosa, C. Lecomte, E. Molins, S. Veintemillas, A. Cousson, W. Paulus, Acta Crystallogr. B52 (1996) 519.
[73] A. Fkyerat, A. Guelzim, F. Baert, W. Paulus, G. Heger, J. Zyss, A. Perigaud, Acta Crystallogr. B51 (1995) 197.
[74] A. Fkyerat, A. Guelzim, F. Baert, J. Zyss, A. Perigaud, Phys. Rev. B 53 (1996) 16236.
[75] M. Souhassou, C. Lecomte, R.H. Blessing, A. Aubry, M.-M. Rohmer, R. Wiest, M. Benard, M. Merraud, Acta Crystallogr. B47 (1991) 253.
[76] F. Hamazaoui, F. Baert, C. Wojcik, Acta Crystallogr. B52 (1996) 159.
[77] A. El-Haouzi, N.K. Hansen, C. Le Henaff, J. Protas, Acta Crystallogr. A52 (1996) 291.
[78] M.A. Spackman, P.G. Byrom, Acta Crystallogr. B53 (1997) 553.
[79] F. Hamazaoui, F. Baert, J. Zyss, J. Mater. Chem. 6 (1996) 1123.
[80] P. Coppens, Phys. Rev. Lett. 34 (1975) 98.